Vortex chain in anisotropic spin-orbit-coupled spin-1 Bose-Einstein condensates

Chao-Fei Liu,[1,2] Yan-Mei Yu,[2] Shih-Chuan Gou,[3] and Wu-Ming Liu[2]

[1]*School of Science, Jiangxi University of Science and Technology, Ganzhou 341000, China*

[2]*Beijing National Laboratory for Condensed Matter Physics, Institute of Physics, Chinese Academy of Sciences, Beijing 100190, China*

[3]*Department of Physics, National Changhua University of Education, Changhua 50058, Taiwan*

We investigate the rotating spin-1 Bose-Einstein condensates with anisotropic spin-orbit coupling by using the damped projected Gross-Pitaevskii equation. The anisotropic spin-orbit coupling can cause some vortices to form the vortex chain, where the vortices link up with each other in a line. The formation of the vortex chain starts from very small rotation frequency and coexists with more remanent vortices with the increasing rotation frequency. By increasing the anisotropy of the spin-orbit coupling, the creation of the vortex chain is enhanced, accompanied by the emergence of several types of vortex chain and other vortex configurations. When the vortices of the $m_F = -1$ and $m_F = +1$ components are of synchronous phases, such vortex configurations do not cause any topological excitation in the spin texture.

I. INTRODUCTION

The Mermin-Ho [1] and Anderson-Toulouse [2] coreless vortices are examples of topological excitations that can be realized in spinor Bose-Einstein condensates (BECs). The difference between the Mermin-Ho vortices and the Anderson-Toulouse vortices comes from the magnetization at the boundary. The axisymmetric Mermin-Ho and Anderson-Toulouse vortices in the spin-1 BECs have been investigated by several authors [3–10]. It was found that the three components ($m_F = 1, 0, -1$), with different phase winding numbers $\langle 0, 1, 2 \rangle$, respectively, are arranged to be effectively phase separated in the radial direction with a concentric structure. Note that the vortex in spin-1 BECs can be described with the phase winding number $\langle a, b, c \rangle$ according to the wave function $(\phi_1, \phi_0, \phi_{-1})$ [3–6]. On the other hand, there are some nonaxisymmetric vortex configurations [5], such as the $\langle 1, 1, 1 \rangle$ vortices and the $\langle 1, 1, -1 \rangle$ vortices. Such configurations have attracted great research interest [3–10] and have motivated further exploration on other possible vortex configurations in spin-1 BECs.

Recent advances of synthetic magnetic fields [spin-orbit (SO) coupling] techniques [11,12] on BECs have stimulated considerable interest in exploring the exotic vortical structures hosted by such systems. For example, Xu *et al.* [13] have found that increasing SO-coupling strength would favor a triangular vortex lattice in fast rotating BECs. Further, the half-quantum vortex lattice is predicted in SO-coupled BECs under rotation if the trapping potential is strong and the interaction is relatively weak [14]. Very recently, Liu *et al.* have found the three-vortex configurations of the vortex lattice in SO-coupled spin-1 BECs [15]. It is interesting to explore how SO coupling produces unknown types of vortex configurations other than the SO coupling effect itself [16–24]. The anisotropic SO-coupled BECs were first discussed in Ref. [25]. With the anisotropic SO coupling, the ground-state phase diagrams are found to have much richer structures than those obtained using mean-field couplings [26]. However, it remains unclear how anisotropic SO coupling affects the vortex configurations in the spin-1 BECs.

Generally speaking, the vortices formed in each component of the spinor BECs have a more or less uniform spatial distribution [13–15,27–31]. It is unusual for some vortices to link up with each other in a line in the BECs. Furthermore, the vortex configurations can induce some topological excitations of the spin texture, such as the skyrmion and the meron [4,6–8]. Liu *et al.* have already shown that the half-skyrmion relates to a special three-vortex structure with SO coupling [15]. The mechanism for the topological excitation of spin texture is not well understood. It is not known whether all the vortex configurations in the spin-1 BECs can induce the nontrivial spin texture. Therefore, a systematical illumination on this subject is desirable.

In this paper, we mainly focus on another special vortex configuration: the vortex chain. In previous investigations, the vortex chain phenomenon has been found in the SO-coupled pseudospin-1/2 BECs [14,23,24]. However, a full understanding on this phenomenon has not been realized. In particular, the structure of the vortex chain in the spin-1 BECs should be more complicated than that in the pseudospin-1/2 BECs. Here, the anisotropic SO coupling is used to induce the vortex chains and other vortex configurations in the rotating spin-1 BECs. We find the vortex chain results from the superposition of the counterpropagating plane-wave phases of BECs. The strength of the anisotropic SO coupling can adjust the structure of the vortex chain as well as other vortex configurations. We develop a method to characterize the vortex configuration according to the winding number, the component of BECs, and the relative position of vortices. Furthermore, our results indicate the condition for the vortex configuration to induce the nontrivial spin texture, such as skymion.

The paper is organized as follows: the damped projected Gross-Pitaevskii equations and some initial condition for our simulations are introduced in Sec. II. In Sec. III we consider various rotation frequencies to produce the vortex chain in the anisotropic SO-coupled spin-1 BECs, and we explain the mechanism of the creation of the vortex chain. In Sec. IV we discuss the effect of anisotropic SO coupling on the vortex chain. In Sec. V a description for characterizing the vortex chain as well as the various vortex configurations is given. In

Sec. VI the relationship between the vortex configuration and the spin texture is systematically explored. A summary of our results is presented in Sec. VII.

II. DAMPED PROJECTED GROSS-PITAEVSKII EQUATION FOR ANISOTROPIC SPIN-ORBIT-COUPLED SPIN-1 CONDENSATES

The dynamics of $F = 1$ spinor BECs with SO coupling can be described by the following coupled nonlinear Schrodinger equations:

$$i\hbar \frac{\partial \Psi_j}{\partial t} = \left[-\frac{\hbar^2 \nabla^2}{2m} + \frac{m\omega^2(x^2+y^2)}{2} + g_n|\Psi|^2 \right] \Psi_j$$
$$+ g_s \sum_{\alpha=x,y,z} \sum_{n,k,l=0\pm 1} (\widehat{F}_\alpha)_{jn}(\widehat{F}_\alpha)_{kl} \Psi_n \Psi_k^* \Psi_l$$
$$- \Omega \widehat{L}_z \Psi_j + \sum_{\alpha=x,y} \sum_{n=0\pm 1} \kappa_\alpha (\widehat{F}_\alpha)_{jn} p_\alpha \Psi_n, \quad (1)$$

where $\Psi_j(j = 0,\pm 1)$ denotes the macroscopic wave function of the atoms condensed in the spin state $|F = 1, m_F = j\rangle$, m the mass of atom, ω the trapped frequency, $\widehat{F}_{\alpha=x,y,z}$ the spin-1 matrices, Ω the rotation frequency, $\widehat{L}_z = -i\hbar(x\partial_y - y\partial_x)$ the z component of the orbital angular momentum, $p_\alpha = -i\hbar\frac{\partial}{\partial\alpha}$ ($\alpha = x,y$) the momentum operator, and κ_α denotes the strength of SO coupling which carries the unit of velocity. Note that the coupling constants $g_n = \frac{4\pi\hbar^2(2a_2+a_0)}{3m}$, $g_s = \frac{4\pi\hbar^2(a_2-a_0)}{3m}$ come from the density-density and spin-exchange interactions, respectively.

Generally, in real experiments the ultracold Bose gases are only partially condensed with the noncondensed thermal cloud which provides a source of dissipation and causes the effect of damping [32,33]. Meanwhile, it is a critical operation to obtain the BECs with the evaporative cooling which can be approximately viewed as a quenching process. Here, we use the damped projected Gross-Pitaevskii equation (PGPE) [34] to describe the quenching process. We note the stochastic PGPE [30,34,35] can describe a quenching process in a finite-temperature BECs. When the "thermal fluctuations" have been removed by the damping effect, a possible energetic ground state would occur. This treatment can be called as the damped PGPE, which has been introduced by Rooney [34] when they have a comparison of the stochastic PGPE, damped PGPE, and PGPE.

The damped PGPE can be obtained by neglecting the noise term according to the corresponding stochastic PGPE [34]. Similarly to the stochastic PGPE, the system is divided into the coherent region with the energies of the state below E_R and the noncoherent region with the energies of the states above E_R. The damped PGPE is written as

$$d\Psi_j = \mathcal{P}\left\{ -\frac{i}{\hbar}\widehat{H}_j\Psi_j dt + \frac{\gamma_j}{k_B T}(\mu - \widehat{H}_j)\Psi_j dt \right\}, \quad (2)$$

where $\widehat{H}_j\Psi_j$ denotes the right-hand-side part of Eq. (1), T the final temperature, k_B the Boltzmann constant, μ the chemical potential, and γ_j the growth rate for the jth component. The projection operator $\mathcal{P}$ is used to restrict the dynamics of the spin-1 BECs in the coherent region. The damped PGPE is equal to the limit case of zero temperature in the stochastic

PGPE. In this scenario, all of the finite-temperature physics normally present in the PGPE theory is lost.

In numerical simulations, we use the spin-1 BECs of ^{87}Rb [36] with $\frac{\gamma_j}{k_B T} = 0.03$ and the trapped frequency $\omega = 200 \times 2\pi$. The unit of length, time, energy, and strength of SO coupling correspond to $\sqrt{\hbar/(m\omega)}$ ($\approx 0.76 \mu$m), ω^{-1} ($\approx 0.8 \times 10^{-3}$ s), $\hbar\omega$, and $\sqrt{\hbar\omega/m}$ ($\approx 0.96 \times 10^{-3}$ m/s), respectively. The initial state of each Ψ_j is generated by sampling the grand-canonical ensemble for a free ideal Bose gas with the chemical potential $\mu_{j,0} = 3.6\hbar\omega$. This sampling would bring some initial thermal noise to break symmetry and give the true energetic ground state once the thermal fluctuations have been removed by the damping. Meanwhile, the condensate band must lie below the energy cutoff $E_R > E_k = \frac{\hbar^2|k|^2}{2m}$. Note that $k = 2\pi(n_x, n_y)/L$, where n_x, n_y are integers and L is the size of the computation domain. Furthermore, the total number of modes is n_x, $n_y = 300$, and the energy cutoff is chosen at n_{xc}, $n_{yc} = 150$. To simulate the quenching process, the final chemical potential of the noncondensate band are altered to the new values $\mu = 25\hbar\omega > \mu_{j,0}(j = 0,\pm 1)$.

III. EFFECT OF ROTATION FREQUENCY ON CREATION OF VORTEX CHAIN IN SPIN-ORBIT-COUPLED SPIN-1 BECS

First, with the fixed SO coupling strengths, $\kappa_x = 1$ and $\kappa_y = 0$, we aim to study the influence of the rotation frequency on the formation of the vortex chain in the spin-1 BECs of ^{87}Rb [36]. We choose $\mu_{j,0}(j = 0,\pm 1) = 3.6\hbar\omega$ and $\mu = 25\hbar\omega$. Figure 1 displays the densities and phases obtained under the equilibrium state with different rotation frequencies. The vortices can be identified in the phase image of each component of the BECs. For the case of the lowest rotation frequency ($\Omega = 0.2\omega$), all the vortices form a line along the x axis and completely traverse the whole BECs [see Fig. 1(a)]. This new interesting configuration is referred to as the vortex chain, which essentially differs from the symmetric and equal distribution of vortices in the rotating BECs. With the rotation frequency $\Omega = 0.3\omega$, more vortices are excited, and there are also several vortices appearing on both sides of the center vortex chain, following a relatively symmetrical distribution [see Fig. 1(b)]. The number of vortices in the off-vortices-chain region increases with the rotation frequency Ω [see Fig. 1(c)]. As compared with the coreless vortices that have been reported in Refs. [4,6–8], the maximum value of the total densities is not at the origin of the coordinate plane. Because of the vortex chain, some local minima of the total densities along the x axis can be distinguished [see the fourth column].

Figure 2 illustrates the position of the vortices shown in Fig. 1. As shown in Fig. 2, the vortices of the $m_F = \pm 1$ components are overlapped in the vortex chain, and the vortices of the $m_F = \pm 1$ components and the vortices of $m_F = 0$ are arranged alternately in a line along the x axis. The vortices of the three components are coupled in the regions off the x axis, consisting of the three-vortex structure [15]. The phase difference shown in Fig. 1(a) tends to be zero, which means that the $m_F = -1$ and $m_F = 1$ components are synchronous when the system reaches the equilibrium state. The phase differences shown in Figs. 1(b) and 1(c) also tends to be zero except
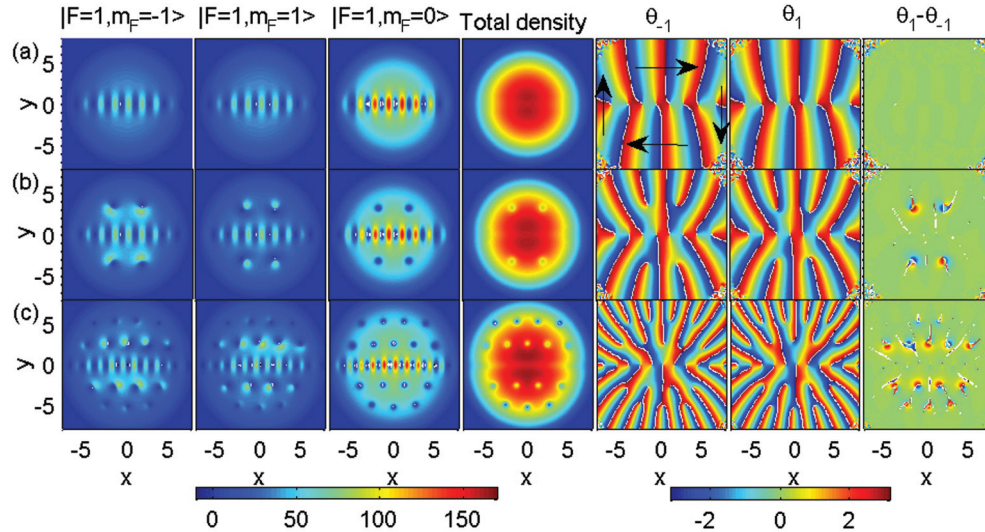
FIG. 1. (Color online) Effect of rotation frequency on the densities and phases of the anisotropic SO-coupled spin-1 BECs of ^{87}Rb when the system reaches the equilibrium state. (a) $\Omega = 0.2\omega$, (b) $\Omega = 0.3\omega$, and (c) $\Omega = 0.5\omega$. Here, $\kappa_x = 1.0$, $\kappa_y = 0$, $a_0 = 101.8a_B$, and $a_2 = 100.4a_B$. Note that the fifth and sixth columns are the phases of $m_F = -1$ and $m_F = 1$ components, respectively. The atom numbers (N_{-1}, N_0, N_1) approximately are $(3.5 \times 10^3, 7.0 \times 10^3, 3.5 \times 10^3)$, $(4.1 \times 10^3, 7.3 \times 10^3, 3.6 \times 10^3)$, and $(4.8 \times 10^3, 9.1 \times 10^3, 4.9 \times 10^3)$, respectively. The length unit and strength of SO coupling are 0.76 μm and 0.96×10^{-3} m/s, respectively.

in the region where the off-x-axis vortices locate. Figure 2 also indicates the patterns of the vortex distributions under the anisotropic SO coupling of $\kappa_x = 1$ and $\kappa_y = 0$. The vortices will first distribute along the x axis as far as they can until the repulsive force between them is so strong that the remaining

vortices prefer to appear on both sides of the x axis in an approximately symmetric manner.

Figure 3 illustrates the profiles of the vortex chain shown in Figs. 1(a)–1(c). As shown in Fig. 3(a), the $m_F = -1$ and $m_F = 1$ components are of the same density profiles along the x axis. When the rotation frequency increases up to 0.3ω, the density profiles of the $m_F = -1$ and $m_F = 1$ components
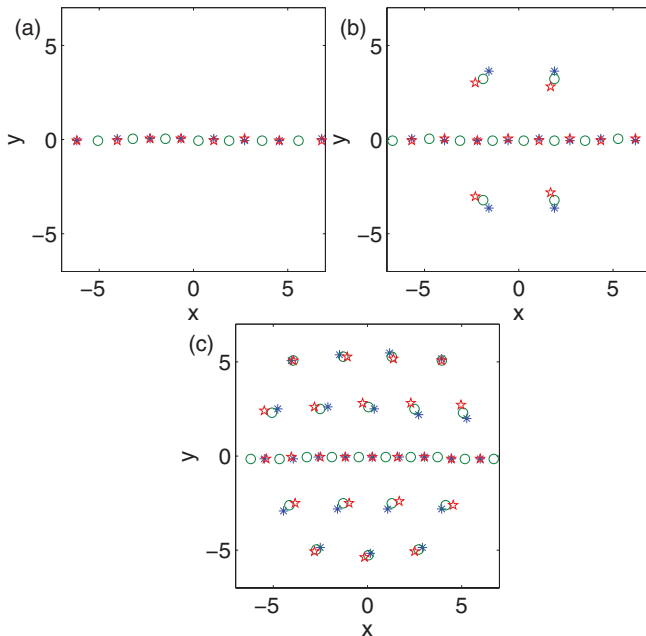

FIG. 2. (Color online) Effect of rotation frequency on the position of vortices in the anisotropic SO-coupled spin-1 BECs of ^{87}Rb in Fig. 1. The asterisks (∗), circles (○), and stars (⋆) are the position of vortices formed by the $m_F = -1$, $m_F = 0$, and $m_F = +1$ components, respectively. (a) $\Omega = 0.2\omega$, (b) $\Omega = 0.3\omega$, and (c) $\Omega = 0.5\omega$. The length unit and strength of SO coupling are 0.76 μm and 0.96×10^{-3} m/s, respectively.
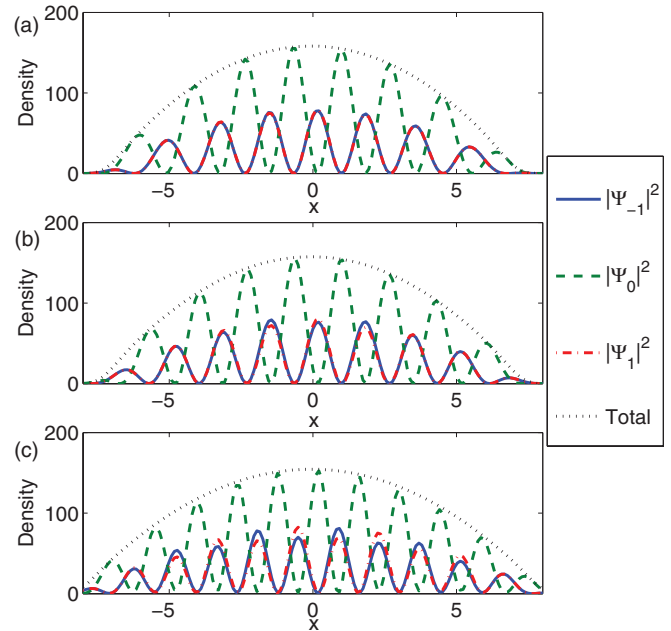

FIG. 3. (Color online) Effect of rotation frequency on the profiles of the vortex chain in the the anisotropic SO-coupled spin-1 BECs of ^{87}Rb in Fig. 1. (a) $\Omega = 0.2\omega$, (b) $\Omega = 0.3\omega$, and (c) $\Omega = 0.5\omega$. The length unit and strength of SO coupling are 0.76 μm and 0.96×10^{-3} m/s, respectively.

tend to differ. Meanwhile, the vortices continuously and homogeneously distribute along the x axis so we have to view them as a whole: the vortex chain. It is obvious that the vortex chain expands over the whole BECs in the three cases in Fig. 1. Furthermore, the numbers of vortices in the three vortex chains increase as the rotation frequency increases. Note that the number of vortices in a chain is finite and intrinsic at the equilibrium state with all the considered parameters. We cannot change the intrinsic number of vortices in the chain artificially unless the parameters are changed. Although the fast rotation can cause larger [37] BECs where more vortices would be stored along the x axis to form the chain, we do not discuss the limit rotation frequency in this study.

The formation of the vortex chain derives from the anisotropic spin-orbit coupling. Similarly to the formation of vortex lattice in the spin-0 scenario, the rotation effect induces the creation of the vortices in the case of the SO-coupled spin-1 BECs. Thus, we observe some lines where the phases change discontinuously from red to blue in the fifth and sixth columns of Fig. 1, which corresponds to the branch cuts between the phases $-\pi$ and π. The ends represent phase defects, i.e., the vortex. All the lines extend to the outskirts of the BEC, where the density of the BEC is almost negligible, and end with another defect which offers neither the energy nor the angular momentum to the system. The additional anisotropic SO coupling terms cause the decrease of the system's energy. The κ_y term in the equation of motion does not affect the system's energy ($\kappa_y = 0$). The energy contributions of the additional anisotropic spin-orbit terms depend on κ_x, which is not zero in the equation of motion. In order to lower more energy, the gradient of phase should remain mainly on the x direction. Therefore, it would cause the plane-wave phase following the x direction if there is no rotation and creation of vortices. In the presence of vortices, the plane-wave phase is changed to form a circle [see the fifth column in Fig. 1(a)] and has to follow the x direction mainly. Thus, the vortices are forced to distribute along the x axis. Therefore, we observe the vortex chain along the x axis with the anisotropic SO coupling ($\kappa_x = 1$, $\kappa_y = 0$) in Fig. 1. For the anisotropic SO coupling with $\kappa_x = 0$ and $\kappa_y = 1$, the vortices distribute along the y axis.

We find that the vortex chain phenomenon occurs even when the rotation frequency is as small as $\Omega = 0.02\omega$. Without rotation, the BECs degenerate into the plane-wave phase [16, 18,19,22] under the equilibrium state. We do not fix the ratio of the three components in the dynamical process, so the mixture ratio of the three components depends on the system itself.

We now give a physical explanation about the vortex chain in the small rotation limit. The vortex chain results from two plane-wave phases with opposite momenta. It is well known that the SO-coupled BECs sustain the plane-wave phase [16,18,19,22]. The phase gradient of the ground state with the plane-wave phase is along the orientation of the SO coupling. The demarcation lines between the discontinuous $-\pi$ and π phases end at the boundary of the BECs, where the densities approach zero. However, when the BECs are rotated, the spatial distribution of phases changes. For the case of isotropic SO coupling, the gradients of the phase encircle the center, following the emergence of the vortices [15]. Figure 4 shows the phase's gradients of the $m_F = -1$ component in
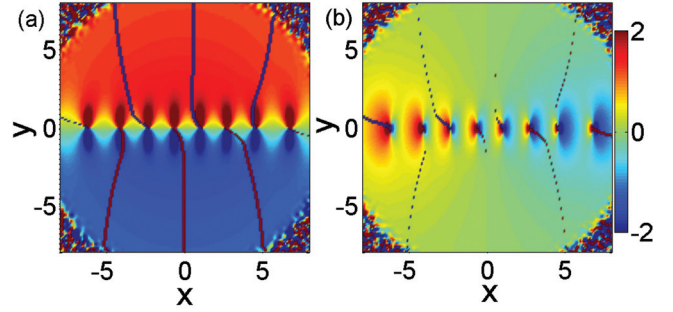

FIG. 4. (Color online) The phase's gradient of $m_F = -1$ component in Fig. 1(a). (a) $\frac{\partial \theta_{-1}}{\partial x}$ and (b) $\frac{\partial \theta_{-1}}{\partial y}$. The length unit and strength of SO coupling are 0.76 μm and 0.96×10^{-3} m/s, respectively.

Fig. 1(a). The curves come from the interface between the values 0 and 2π. The value of $\frac{\partial \theta_{-1}}{\partial x}$ does not approach 0, and $\frac{\partial \theta_{-1}}{\partial y}$ approaches 0 in the off-x-axis region. Instead, the properties of $\frac{\partial \theta_{-1}}{\partial x}$ approach 0 and $\frac{\partial \theta_{-1}}{\partial y}$ does not approach 0 along the x axis. This indicates that the gradients of the phase mainly continue in the same direction and the counterdirection of the anisotropic SO coupling. The phases form a whole circle as the arrows indicate in Fig. 1(a) (the fifth column). The demarcation lines between the discontinuous $-\pi$ and π phases then have to start from the domain wall of the two opposite plane-wave phases and end at the outskirts of the BECs. Therefore, the vortex chain occurs although the rotation frequency is very low.

IV. EFFECT OF STRENGTH OF ANISOTROPIC SPIN-ORBIT COUPLING ON THE VORTEX CHAIN

We now consider the influence of the strength of the anisotropic SO coupling on the vortex chain. The rotation frequency is fixed to be $\Omega = 0.5\omega$, and all other parameters are the same with Fig. 1 except the strength of the anisotropic SO coupling. Figure 5(a) indicates that no vortex chain is obtained for $\kappa_x = 0.1$ and $\kappa_y = 0$. Several vortices of the $m_F = -1, 0, 1$ components appear along the x axis for $\kappa_x = 0.5$ and $\kappa_y = 0$, as shown in Fig. 5(b). The phase difference in the seventh column shows that there is no synchronization of the phases. The vortex chains become clearer for each component for $\kappa_x = 1.5$ and $\kappa_y = 0$, as shown in Fig. 5(c), and the phase difference along the x axis is zero. In addition to the vortices on the x axis, other vortices distribute approximately parallel to the x axis. The phase difference of the off-x-axis vortices near $y = \pm 5$ approaches 0. This differs from those near the $y = \pm 2.5$ region. These results indicate that the stronger the anisotropic SO coupling, the more the regions of the $m_F = -1$ and $m_F = 1$ components tend to evolve synchronously.

Figure 6 shows the corresponding vortex positions in Fig. 5. It further displays the effect of the anisotropic SO coupling on the vortices. Figure 6(a) indicates that the relatively weak anisotropic SO coupling ($\kappa_x = 0.1$ and $\kappa_y = 0$) indeed cannot induce the vortex chain in Fig. 5(a). Figure 6(b) shows a vortex chain where the vortices of the $m_F = -1$ component do not overlap with those of the $m_F = 1$ component in Fig. 5(b). Furthermore, except the vortex chain along the x axis, all other vortices form the three-vortex structure, just as that in Ref. [15].
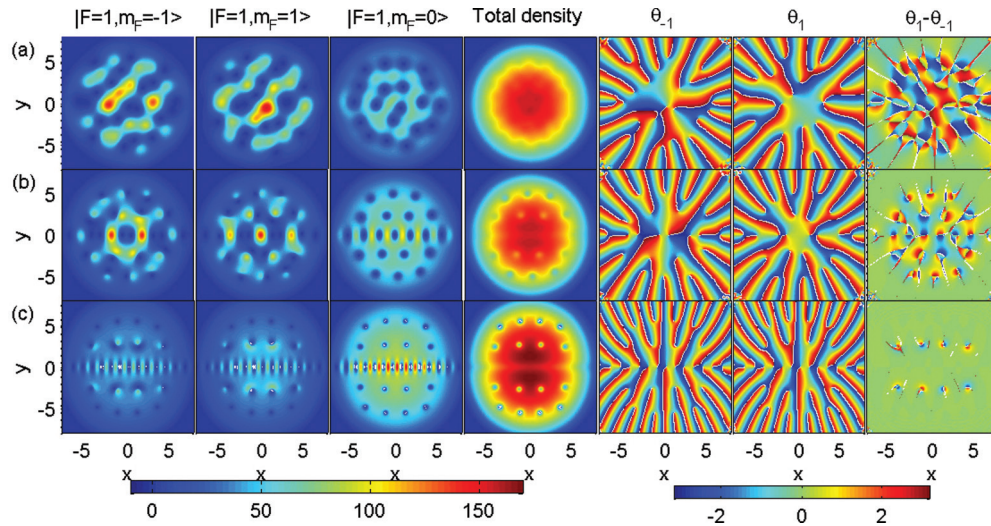
FIG. 5. (Color online) Effect of anisotropic SO coupling on the densities and phases of the rotating spin-1 BECs of ^{87}Rb when the system reaches the equilibrium state. (a) $\kappa_x = 0.1$ and $\kappa_y = 0$. (b) $\kappa_x = 0.5$ and $\kappa_y = 0$. (c) $\kappa_x = 1.5$ and $\kappa_y = 0$. Here $\Omega = 0.5\omega$, $a_0 = 101.8a_B$, and $a_2 = 100.4a_B$. Note that the fifth and sixth columns are the phases of $m_F = -1$ and $m_F = 1$ components, respectively. The atom numbers (N_{-1}, N_0, N_1) approximately are $(5.4 \times 10^3, 5.3 \times 10^3, 5.5 \times 10^3)$, $(4.9 \times 10^3, 7.5 \times 10^3, 4.8 \times 10^3)$, and $(5.2 \times 10^3, 1.05 \times 10^4, 5.4 \times 10^3)$, respectively. The length unit and strength of SO coupling are 0.76 μm and 0.96×10^{-3} m/s, respectively.

Figure 6(c) indicates that the vortex chain in Fig. 5(c) is similar to that in Fig. 1. The anisotropic SO coupling can cause the vortices of different components to overlap with each other. The off-x-axis vortices near $y = \pm 5$ completely overlap, but the off-x-axis vortices near $y = \pm 2.5$ do not. Such a difference is because of the different densities at $y = \pm 5$ and $y = \pm 2.5$.

In fact, this effect is caused by the trap potential, strength of SO coupling, and so on. Near the center, the density is bigger than that at the boundary. When the three vortices overlap, it will offer more energy and angular momentum to the system. Thus, the completely overlapped three vortices easily appear at the boundary of the BECs (low-density region).

The density profiles along the x axis are plotted in Fig. 7. The vortex chain indeed does not occur along the x axis in
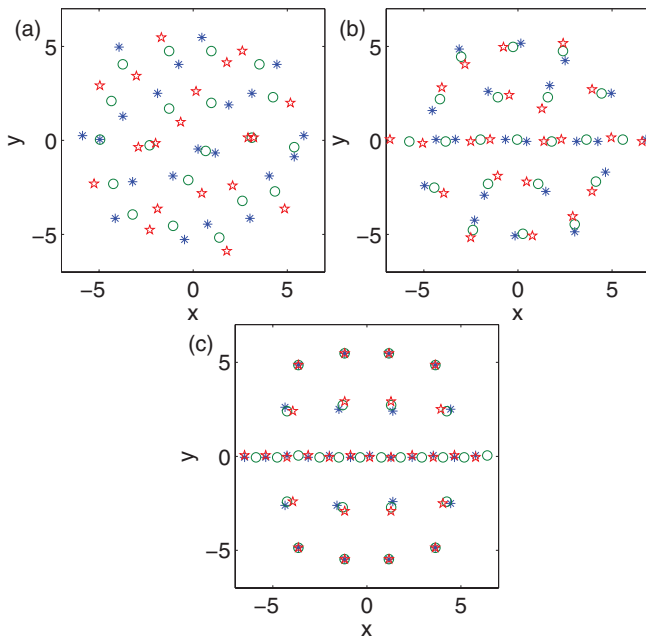

FIG. 6. (Color online) Effect of anisotropic SO coupling on the position of vortices in the rotating spin-1 BECs of ^{87}Rb in Fig. 5. The asterisks (∗), circles (◦) and stars (⋆) denote the position of vortices formed by the $m_F = -1$, $m_F = 0$, and $m_F = +1$ components, respectively. (a) $\kappa_x = 0.1$ and $\kappa_y = 0$. (b) $\kappa_x = 0.5$ and $\kappa_y = 0$. (c) $\kappa_x = 1.5$ and $\kappa_y = 0$. The length unit and strength of SO coupling are 0.76 μm and 0.96×10^{-3} m/s, respectively.
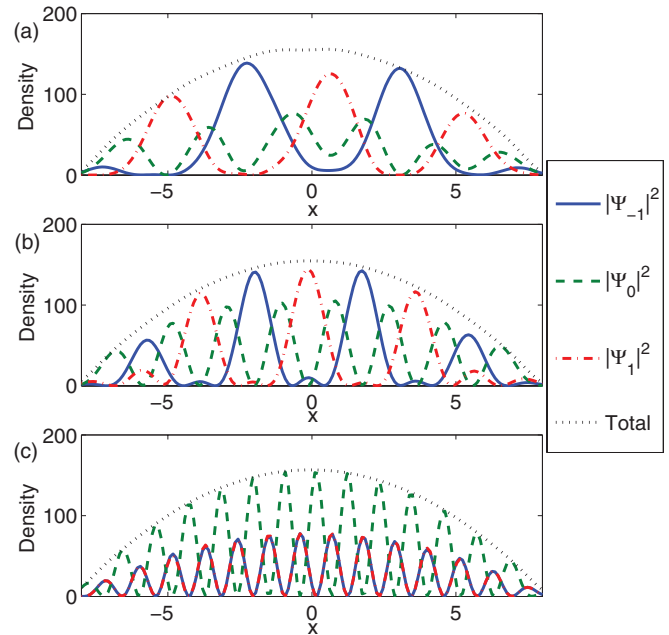

FIG. 7. (Color online) Effect of anisotropic SO coupling on the profiles of vortex chain in the rotating spin-1 BECs of ^{87}Rb in Fig. 5. (a) $\kappa_x = 0.1$ and $\kappa_y = 0$. (b) $\kappa_x = 0.5$ and $\kappa_y = 0$. (c) $\kappa_x = 1.5$ and $\kappa_y = 0$. The length unit and strength of SO coupling are 0.76 μm and 0.96×10^{-3} m/s, respectively.
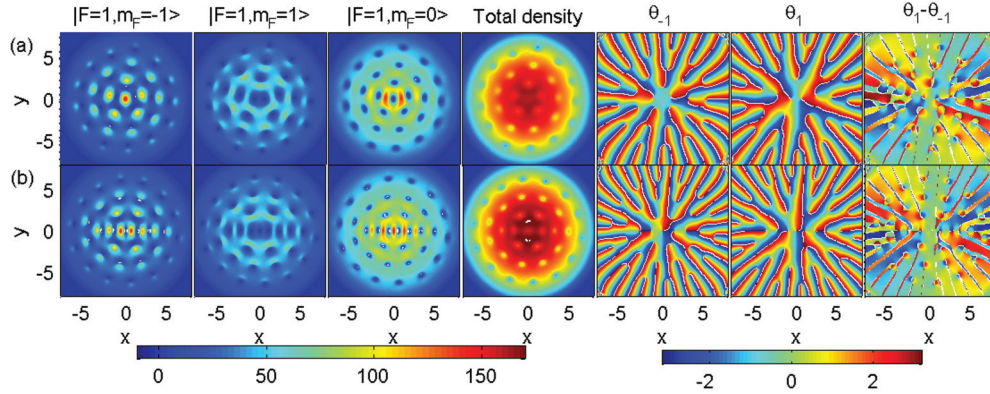
FIG. 8. (Color online) Effect of anisotropic SO coupling on the densities and phases of the rotating spin-1 BECs of ^{87}Rb when the system reaches the equilibrium state. (a) $\kappa_x = 1.0$ and $\kappa_y = 0.7$. (b) $\kappa_x = 1.5$ and $\kappa_y = 1.2$. Here $\Omega = 0.5\omega$, $a_0 = 101.8a_B$, and $a_2 = 100.4a_B$. Note that the fifth and sixth columns are the phases of the $m_F = -1$ and $m_F = 1$ components, respectively. The atom numbers (N_{-1}, N_0, N_1) approximately are $(4.7 \times 10^3, 9.4 \times 10^3, 5.6 \times 10^3)$ and $(5.5 \times 10^3, 1.12 \times 10^4, 6.1 \times 10^3)$, respectively. The length unit and strength of SO coupling are 0.76 μm and 0.96×10^{-3} m/s, respectively.

Fig. 5(a), because some minimum values in Fig. 7(a) do not approach zero at all. Figure 7(b) indicates that the minimum values of the three components are separated from each other. When SO coupling of κ_x is up to 1.5, the property of the density profiles is similar to that in Fig. 3, where the density profiles of the $m_F = -1$ and $m_F = 1$ components are equal in Fig. 7(c). According to the results of Figs. 3 and 7, we can conclude that the anisotropic SO coupling tends to equalize the density profiles of the $m_F = -1$ and $m_F = 1$ components in the vortex chain, but the fast rotation effect causes the slight deviation.

Further, the formation of the vortex configuration is investigated for different κ_y with the other parameters being the same with Figs. 1(c) and 5(c), respectively, in order to explain the influence of κ_y on the vortex chains. As shown in Figs. 8(a) and 9(a), the vortex chain is not observed for $\kappa_y = 0.7$, whereas in Figs. 8(b) and 9(b), the vortex chain is observed for $\kappa_y = 1.2$. Figure 9(c) further plots the density profile of the vortex chain in Fig. 8(b). By comparing Fig. 9(c) with Figs. 3 and 7, the total density profile is not smooth. Meanwhile, the vortex chain locates at the center of the BECs, not traversing the whole BECs. Therefore, not only κ_x but also κ_y of the anisotropic SO coupling can control the formation of the vortex chain.

We have also performed simulations with the antiferromagnetic BECs of ^{23}Na, where $g_s > 0$. We find that the vortex chain phenomenon can occur as long as the anisotropic SO coupling of κ_x ($\kappa_y = 0$) is strong enough. Compared with Ref. [24], which also uses the anisotropic SO coupling, the mechanism for obtaining the vortex chain is the same. However, the structure of the vortex chain in the spin-1 BECs is indeed more complicated than that in the pseudospin-1/2 BECs, where the vortices interlacedly array to form a chain.

V. VORTEX CHAINS AND THE RELATED VORTEX CONFIGURATION

Figures 1–9 have shown the vortex chain phenomena induced by the anisotropic SO coupling in spin-1 BECs, where the vortex chain is always accompanied by various

vortex configurations. In Refs. [3,5], vortices are characterized by the winding numbers of three components $(\psi_1, \psi_0, \psi_{-1})$, when the vortex number of each component is no more than 1. However, this characterization is not appropriate to describe the vortex chains in this paper. For characterizing the vortex configuration more conveniently, we write down the winding numbers for every component, and at the same time we use the subscript 1 to denote that the vortices overlaps completely, i.e., the minima of the density profile of the $(\psi_1, \psi_0, \psi_{-1})$ components are at the same position, and the subscript 3 if the minimum density region of the three vortices is completely separated. For example, in this way, we characterize the Mermin-Ho and Anderson-Toulouse coreless
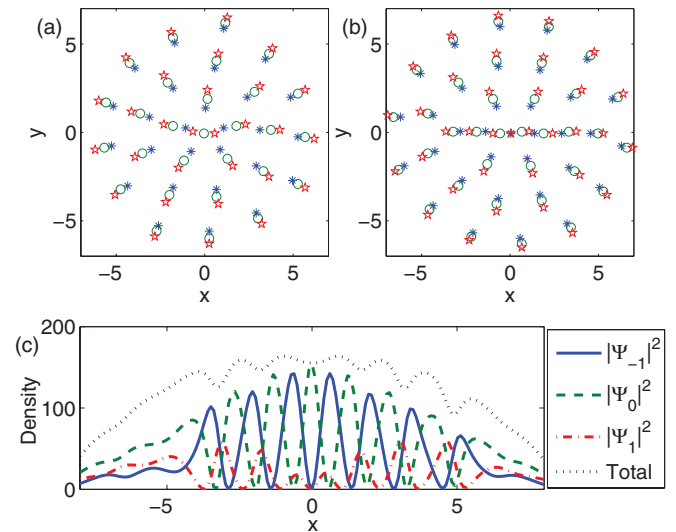

FIG. 9. (Color online) (a) The position of vortices in rotating spin-1 BECs of ^{87}Rb in Fig. 8(a). The asterisks (∗), circles (○), and stars (⋆) are the position of vortices formed by the $m_F = -1$, $m_F = 0$, and $m_F = +1$ components, respectively. (b) The position of vortices in rotating spin-1 BECs of ^{87}Rb in Fig. 8(b). (c) The profile of vortex chain in Fig. 8(b). The length unit and strength of SO coupling are 0.76 μm and 0.96×10^{-3} m/s, respectively.

vortices as $(1_0,2_{-1})_1$ or $(0_1,1_0,2_{-1})_1$ [3,5], where, in the bracket, 0_1 denotes the $m_F = 1$ vortex with winding number 0, 1_0 denotes the $m_F = 0$ vortex with winding number 1, 2_{-1} denotes the $m_F = -1$ vortex with winding number 2, and the subscript 1 out the bracket means that the two vortices overlap. In addition, the nonaxisymmetric $\langle 1,1,1 \rangle$ vortices in Refs. [3,5] can be presented as $(1_1,1_0,1_{-1})_3$, i.e., the three components contain a vortex with winding number 1, respectively, and they locate at three separated positions. Likewise, we characterize the three-vortex structure reported in Ref. [15] as $\langle 1_{-1},1_0,1_1 \rangle_3$. We use the angle brackets (parenthesis) to indicate the vortices, where the total density has (does not have) a local minimum at the region of the vortices.

With this description, the vortex chain in Figs. 1(a)–1(c) and 3(c) can be characterized by $\langle\langle 1_{-1},1_1 \rangle_1,1_0 \rangle_2 \times n$, where the overlapped vortices of the $m_F = -1$ and $m_F = 1$ components are denoted by $\langle 1_{-1},1_1 \rangle_1$. The separation of the $\langle 1_{-1},1_1 \rangle_1$ vortices and the 1_0 vortices is described by the subscript 2, and $\times n$ denotes that there are n $\langle\langle 1_{-1},1_1 \rangle_1,1_0 \rangle_2$ vortex configurations linking one after another to form a chain. The vortex chain in Fig. 5(b) can be written as $[\langle 1_1,1_0,1_1 \rangle_3 + \langle 1_{-1},1_0,1_{-1} \rangle_3] \times n$.

The off-x-axis vortex configuration in Fig. 2(b) can be presented as the $\langle 1_{-1},1_0,1_1 \rangle_3$ vortices. In Fig. 6(c), the vortex configuration near $y = \pm 5$ can be written as the $\langle 1_{-1},1_0,1_1 \rangle_1$ vortices, due to the minimum densities of the three components located at the same position. Generally, the total density profile always tends to be nonsingular and continuous although the vortices occur in the spin-1 BECs [30]. However, the $\langle 1_{-1},1_0,1_1 \rangle_1$ vortices are an unusual case, behaving like a singular vortex in the single-component BEC.

Our results show that the phases of the $m_F = -1$ and $m_F = 1$ components always tend to be synchronous in the developed vortex-chain structure, such as the $\langle\langle 1_{-1},1_1 \rangle_1,1_0 \rangle_2 \times n$ vortex chain obtained by the combination of anisotropic SO coupling and rotation shown in Figs. 1(a)–1(c), 2(a)–2(c), 5(c), and 6(c). Even in the region near such developed vortex chains, where the vortex configuration can be described by the $\langle 1_{-1},1_0,1_1 \rangle_1$ vortices, the phases of the $m_F = -1$ and $m_F = 1$ components also tend to be synchronous, which is shown in Figs. 2(c) and 6(c). As shown in Fig. 6, as κ_x increases from 0.5 to 1.5, the formation of the vortex chain is changed noticeably, where $[\langle 1_1,1_0,1_1 \rangle_3 + \langle 1_{-1},1_0,1_{-1} \rangle_3] \times n$ vortex structure develops into the $\langle\langle 1_{-1},1_1 \rangle_1,1_0 \rangle_2 \times n$ vortex chains. As we have already known, the vortices of different components usually are not overlapped, which is energetically favorable, when the SO coupling interaction is absent. We find that κ_y also influences the formation of the vortex chains through comparing Figs. 6(c) and 9(b). With the same κ_x as Fig. 6, κ_y is increased to 1.2 in Fig. 9(b); therefore, the anisotropy in the x direction becomes weaker in Fig. 9(b) as compared with Figs. 6(c). Due to the decreased anisotropy, we find that the vortex chain is fragmented, which is described by $\langle 1_1,1_0,1_{-1} \rangle_3 \times 2 + \langle 1_1,1_0 \rangle_2 + \langle 1_{-1},1_1 \rangle_1 + \langle 1_0,1_1 \rangle_2 + \langle 1_{-1},1_0,1_1 \rangle_3 \times 2$. Correspondingly, the $\langle 1_{-1},1_0,1_1 \rangle_1$ vortices configurations become the $\langle 1_{-1},1_0,1_1 \rangle_3$ configurations, where the phases of the $m_F = -1$ and $m_F = 1$ components around the vortices tends to be nonsynchronous. For clarity, we summarize the results in Table I. The first column shows the strength of anisotropic SO coupling and the rotation frequency, the second column indicates the characterization of the vortex chain, the third column shows some other vortex configurations, and the fourth column shows the figures where the vortex chain appears.

Similarly, the vortex chain in the pseudospin-1/2 BECs [14,24] can be approximately presented by $\langle 1_\uparrow,1_\downarrow \rangle_2 \times n$. In Ref. [23], Radić *et al.* solve the dimensionless GP equations [Eqs. (22)] and obtain the vortex chain (the line of vortices) along the x axis, where the total density at minima is close to but not exactly equal to zero. This property implies the vortex formed by the two condensates should overlap with each other. So the chain can be written as $\langle 1_\uparrow,1_\downarrow \rangle_1 \times n$. Our dynamical Eqs. (1) uses the anisotropic SO coupling on the x-y plane, where the σ_z term and the spatially dependent $\delta(y)$ term have not been considered as in Ref. [23]. Therefore, our results concerning vortex chain differ from those in Ref. [23].

VI. SPIN TEXTURE OF THE VORTEX CHAIN

Usually, the vortex configuration can cause some topological excitation of the spin texture. The spin texture [6–8] is defined by

$$\mathbf{S}_\alpha = \sum_{m,n=0,\pm 1} \Psi_m^* (\widehat{F}_\alpha)_{m,n} \Psi_n / |\Psi|^2 \quad (\alpha = x,y,z), \quad (3)$$

and the topological charge density is defined by $q(r) = \frac{1}{4\pi} \mathbf{s} \cdot (\frac{\partial \mathbf{S}}{\partial x} \times \frac{\partial \mathbf{S}}{\partial y})$, where $\mathbf{s} = \mathbf{S}/|\mathbf{S}|$. Since we have introduced the vortex chain excitation, we want to further explore the corresponding spin texture. In order to investigate the topological excitation of the vortex chain, we check the spin texture of the vortex chains and vortex configurations obtained by various cases. As shown in Fig. 10(a), which corresponds to Fig. 5(b) under a small anisotropy SO coupling ($\kappa_x = 0.5$, $\kappa_y = 0$), where the obtained vortex chain is described by $[\langle 1_1,1_0,1_1 \rangle_3 + \langle 1_{-1},1_0,1_{-1} \rangle_3] \times n$, we find that the $\langle 1_1,1_0,1_1 \rangle_3$ vortex configuration relates to the circular skyrmion, while the $\langle 1_{-1},1_0,1_{-1} \rangle_3$ vortex configuration relates to the hyperbolic skyrmion. Figure 10(b) corresponds to Fig. 5(c) under a large anisotropy ($\kappa_x = 1.5$, $\kappa_y = 0$), and Figure 10(c) is the corresponding topological charge density. Being described by $\langle\langle 1_{-1},1_1 \rangle_1,1_0 \rangle_2 \times n$, the obtained vortex chain is more developed and induces the domain of the two counterorientation arrows of the spin texture. In the regions of the $\langle 1_{-1},1_0,1_1 \rangle_3$ vortices, we find the half-skyrmion and the nonzero topological charge densities, which is consistent with the previously reported three-vortex configuration in the isotropic SO-coupled spin-1 BECs [15]. No spin texture is found for the $\langle\langle 1_{-1},1_1 \rangle_1,1_0 \rangle_2 \times n$ vortex chain, and the topological charge density is around zero in the region of the vortex chain and the $\langle 1_{-1},1_0,1_1 \rangle_1$ vortices, which coincides with the general cases whereby $\langle 1_{-1},1_0,1_1 \rangle_1$ vortices usually do not cause nontrivial topological excitation. These properties indicate that the entire vortex configuration cannot induce the nontrivial spin texture. Figure 10(d) is the spin texture of vortex chain obtained in Fig. 8(b) ($\kappa_x = 1.5$, $\kappa_y = 1.2$), which corresponds to an intermediate strength of anisotropy, as compared with Figs. 10(a) and 10(b). Some half-skyrmion structure caused by $\langle 1_{-1},1_0,1_1 \rangle_3$ vortices prevails, instead of the domain wall of the opposite arrows obtained in Fig. 10(b) for the larger anisotropy. The results shown in Fig. 10 indicate the relationship between the vortex configuration and the spin

TABLE I. A summary of the results in above text. The first column indicates the parameters, the second column shows the characterization of the vortex chain, the third column shows some other vortex configurations, and the fourth column indicates the pictures where the results appear.

	Vortex chain	Other vortex configuration	Where
$(\kappa_x = 1, \kappa_y = 0)_{\Omega=0.2\omega}$	$\langle\langle 1_{-1}, 1_1\rangle_1, 1_0\rangle_2 \times n$	No	Fig. 1(a)
$(\kappa_x = 1, \kappa_y = 0)_{\Omega=0.3\omega}$	$\langle\langle 1_{-1}, 1_1\rangle_1, 1_0\rangle_2 \times n$	$\langle 1_{-1}, 1_0, 1_1\rangle_3$	Fig. 1(b)
$(\kappa_x = 1, \kappa_y = 0)_{\Omega=0.5\omega}$	$\langle\langle 1_{-1}, 1_1\rangle_1, 1_0\rangle_2 \times n$	$\langle 1_{-1}, 1_0, 1_1\rangle_3, \langle 1_{-1}, 1_0, 1_1\rangle_1$	Fig. 1(c)
$(\kappa_x = 0.1, \kappa_y = 0)_{\Omega=0.5\omega}$	No vortex chain	$\langle 1_{-1}, 1_0, 1_1\rangle_3, \langle 1_1, 1_0, 1_1\rangle_3, \langle 1_{-1}, 1_0, 1_{-1}\rangle_3$	Fig. 5(a)
$(\kappa_x = 0.5, \kappa_y = 0)_{\Omega=0.5\omega}$	$[\langle 1_1, 1_0, 1_1\rangle_3 + \langle 1_{-1}, 1_0, 1_{-1}\rangle_3] \times n$	$\langle 1_{-1}, 1_0, 1_1\rangle_3$	Fig. 5(b)
$(\kappa_x = 1.5, \kappa_y = 0)_{\Omega=0.5\omega}$	$\langle\langle 1_{-1}, 1_1\rangle_1, 1_0\rangle_2 \times n$	$\langle 1_{-1}, 1_0, 1_1\rangle_3, \langle 1_{-1}, 1_0, 1_1\rangle_1$	Fig. 5(c)
$(\kappa_x = 1, \kappa_y = 0.7)_{\Omega=0.5\omega}$	No vortex chain	$\langle 1_{-1}, 1_0, 1_1\rangle_3$	Fig. 8(a)
$(\kappa_x = 1.5, \kappa_y = 1.2)_{\Omega=0.5\omega}$	$\langle 1_1, 1_0, 1_{-1}\rangle_3 \times 2 + \langle 1_1, 1_0\rangle_2 + \langle 1_{-1}, 1_1\rangle_1 + \langle 1_0, 1_1\rangle_2 + \langle 1_{-1}, 1_0, 1_1\rangle_3 \times 2$	$\langle 1_{-1}, 1_0, 1_1\rangle_3$	Fig. 8(b)

texture. When the phases of vortices formed by the $m_F = -1$ and $m_F = 1$ components are synchronous, the vortex configuration does not induce the nontrivial topological excitation of the spin texture. This means that we must ensure that the corresponding vortex excitation of the $m_F = -1$ and $m_F = +1$ components not to overlap in order to produce some topological excitation of spin texture such as skyrmion.
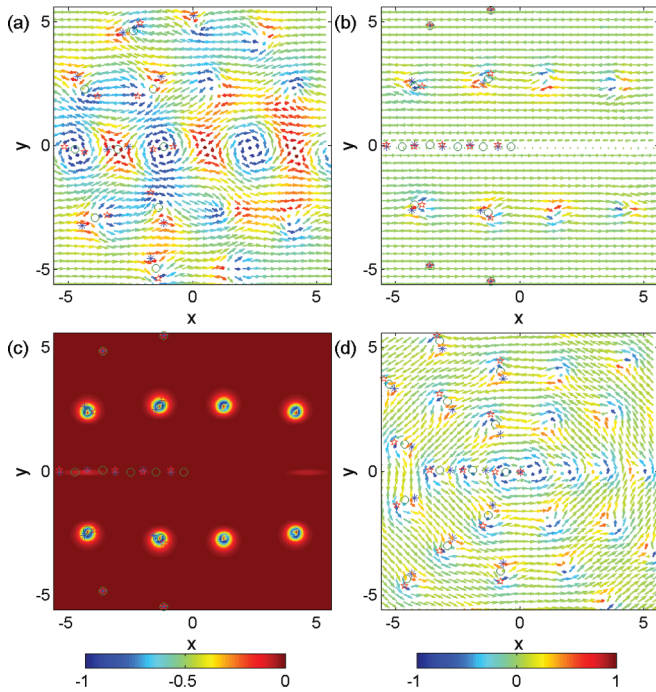

FIG. 10. (Color online) (a) Vortex position and spin texture of spin-1 BECs of ^{87}Rb in Fig. 5(b), where $\kappa_x = 0.5$, $\kappa_y = 0$, and $\Omega = 0.5\omega$. The color of each arrow indicates the magnitude of S_z. The asterisks (∗), circles (◦) and stars (⋆) mark the position of vortices formed by the $m_F = -1$, $m_F = 0$, and $m_F = +1$ components, respectively. Noting that we only mark the vortices in $x < 0$ region in order to illuminate the spin texture and position of vortices clearly. (b) Vortex position and spin texture of spin-1 BEC of ^{87}Rb in Fig. 5(c), where $\kappa_x = 1.5$, $\kappa_y = 0$, and $\Omega = 0.5\omega$. (c) Topological charge density and vortex position in Fig. 5(c). (d) Vortex position and spin texture of spin-1 BEC of ^{87}Rb in Fig. 8(b), where $\kappa_x = 1.5$, $\kappa_y = 1.2$, and $\Omega = 0.5\omega$. The length unit and strength of SO coupling are 0.76 μm and 0.96×10^{-3} m/s, respectively.

Figure 11(a) enlarges the spin texture which is induced by the vortex chain $\langle\langle 1_{-1}, 1_1\rangle_1, 1_0\rangle_2 \times n$ in Fig. 10(b). It is a domain wall between two groups of opposite arrows. According to Fig. 7(c), the density profiles of the $m_F = -1$ and $m_F = 1$ components are equal, and the density difference of the $m_F = -1$ and $m_F = 1$ components corresponds to the S_z vector of the spin texture. We find the spin texture can be presented by

$$\mathbf{S}_{xc} = \tanh[c_1(y + c_2)], \quad \mathbf{S}_{yc} = 0, \quad \mathbf{S}_{zc} = 0. \quad (4)$$

Figure 11(b) is the result with Eq. (3), where $c_1 = -2.5$ and $c_2 = 0.05$. We find that Eq. (3) can well describe the spin texture induced by the vortex chain $\langle\langle 1_{-1}, 1_1\rangle_1, 1_0\rangle_2 \times n$ through
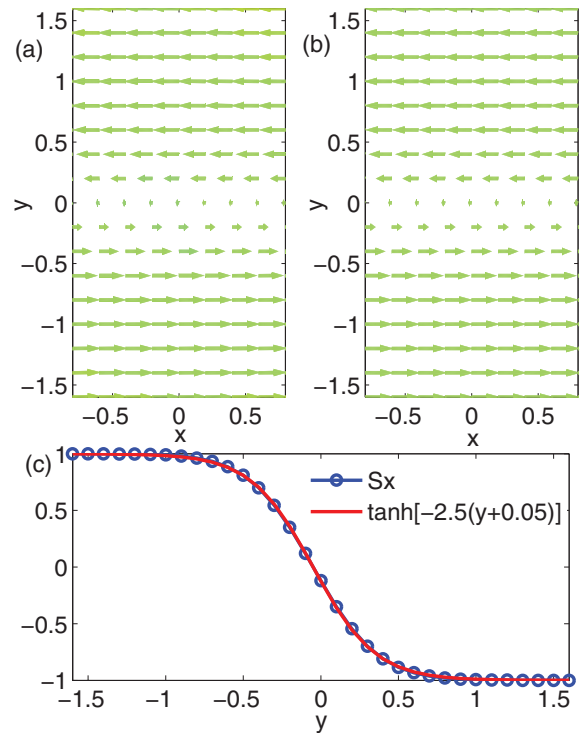

FIG. 11. (Color online) (a) The enlarged spin texture in Fig. 10(b). (b) The spin texture with Eqs. (3), where $c_1 = -2.5$ and $c_2 = 0.05$. (c) A comparison between the spin vector $\mathbf{S}_x$ and the function $\tanh[-2.5(y + 0.05)]$ along the y axis.

comparison of Fig. 11(a) and Fig. 11(b) and comparison of the spin vector $\mathbf{S}_x$ with the function $\tanh[-2.5(y+0.05)]$ along the y axis shown in Fig. 11(c).

VII. CONCLUSION

We have investigated SO-coupled spin-1 BECs under the rotation by using damped PGPE. The anisotropic SO coupling causes the vortex chains and some special vortex configurations such as the $\langle 1_{-1}, 1_0, 1_1 \rangle_1$ vortices. The vortex chains are found to be the consequences of the domain wall of two opposite plane-wave phases. The rotation effect mainly affects the number of vortices in the vortex chain. The isotropy of SO coupling destroys the vortex chain and causes the vortex chain to degenerate into the $\langle 1_{-1}, 1_0, 1_1 \rangle_3$ vortices. Furthermore, our study systematically illuminates the relationship between the vortex configuration and the nontrivial spin texture. We find that the vortex configurations do not relate to some topological excitation of spin texture when the phases of the vortices formed by the $m_F = -1$ and $m_F = +1$ components are synchronous. This study provides exciting perspectives for nonlinear physics of condensates in artificially induced non-Abelian gauge fields.

[1] N. D. Mermin and T. L. Ho, Phys. Rev. Lett. **36**, 594 (1976).

[2] P. W. Anderson and G. Toulouse, Phys. Rev. Lett. **38**, 508 (1977).

[3] T. Isoshima and K. Machida, Phys. Rev. A **66**, 023602 (2002).

[4] T. Mizushima, K. Machida, and T. Kita, Phys. Rev. Lett. **89**, 030401 (2002).

[5] T. Mizushima, K. Machida, and T. Kita, Phys. Rev. A **66**, 053610 (2002).

[6] T. Mizushima, N. Kobayashi, and K. Machida, Phys. Rev. A **70**, 043613 (2004).

[7] K. Kasamatsu, M. Tsubota, and M. Ueda, Phys. Rev. Lett. **93**, 250406 (2004).

[8] K. Kasamatsu, M. Tsubota, and M. Ueda, Phys. Rev. A **71**, 043611 (2005).

[9] L. S. Leslie, A. Hansen, K. C. Wright, B. M. Deutsch, and N. P. Bigelow, Phys. Rev. Lett. **103**, 250401 (2009).

[10] J. Y. Choi, W. J. Kwon, and Y. I. Shin, Phys. Rev. Lett. **108**, 035301 (2012).

[11] Y. J. Lin, R. L. Compton, K. Jiménez-García, J. V. Porto, and I. B. Spielman, Nature (London) **462**, 628 (2009).

[12] Y. J. Lin, K. Jiménez-García, and I. B. Spielman, Nature (London) **471**, 83 (2011).

[13] X. Q. Xu and J. H. Han, Phys. Rev. Lett. **107**, 200401 (2011).

[14] X. F. Zhou, J. Zhou, and C. Wu, Phys. Rev. A **84**, 063624 (2011).

[15] C. F. Liu and W. M. Liu, Phys. Rev. A **86**, 033602 (2012).

[16] C. Wang, C. Gao, C. M. Jian, and H. Zhai, Phys. Rev. Lett. **105**, 160403 (2010).

[17] C. Wu, I. Mondragon-Shem, and X. F. Zhou, Chin. Phys. Lett. **28**, 097102 (2011).

[18] S. Sinha, R. Nath, and L. Santos, Phys. Rev. Lett. **107**, 270401 (2011).

[19] T. L. Ho and S. Z. Zhang, Phys. Rev. Lett. **107**, 150403 (2011).

[20] H. Hu, B. Ramachandhran, H. Pu, and X. J. Liu, Phys. Rev. Lett. **108**, 010402 (2012).

[21] B. Ramachandhran, B. Opanchuk, X. J. Liu, H. Pu, P. D. Drummond, and H. Hu, Phys. Rev. A **85**, 023606 (2012).

[22] S. W. Su, I. K. Liu, Y. C. Tsai, W. M. Liu, and S. C. Gou, Phys. Rev. A **86**, 023601 (2012).

[23] J. Radić, T. A. Sedrakyan, I. B. Spielman, and V. Galitski, Phys. Rev. A **84**, 063604 (2011).

[24] C. F. Liu, H. Fan, Y. C. Zhang, D. S. Wang, and W. M. Liu, Phys. Rev. A **86**, 053616 (2012).

[25] T. D. Stanescu, B. Anderson, and V. Galitski, Phys. Rev. A **78**, 023616 (2008).

[26] T. Ozawa and G. Baym, Phys. Rev. A **85**, 013612 (2012).

[27] E. J. Mueller and T. L. Ho, Phys. Rev. Lett. **88**, 180403 (2002).

[28] T. Kita, T. Mizushima, and K. Machida, Phys. Rev. A **66**, 061601 (2002).

[29] R. Barnett, S. Mukerjee, and J. E. Moore, Phys. Rev. Lett. **100**, 240405 (2008).

[30] S. W. Su, C. H. Hsueh, I. K. Liu, T. L. Horng, Y. C. Tsai, S. C. Gou, and W. M. Liu, Phys. Rev. A **84**, 023601 (2011).

[31] V. Schweikhard, I. Coddington, P. Engels, S. Tung, and E. A. Cornell, Phys. Rev. Lett. **93**, 210403 (2004).

[32] S. Choi, S. A. Morgan, and K. Burnett, Phys. Rev. A **57**, 4057 (1998).

[33] A. A. Penckwitt, R. J. Ballagh, and C. W. Gardiner, Phys. Rev. Lett. **89**, 260402 (2002).

[34] S. J. Rooney, A. S. Bradley, and P. B. Blakie, Phys. Rev. A **81**, 023630 (2010).

[35] A. S. Bradley, C. W. Gardiner, and M. J. Davis, Phys. Rev. A **77**, 033616 (2008).

[36] F. Zhou, Phys. Rev. Lett. **87**, 080401 (2001).

[37] C. H. Hsueh, T. L. Horng, S. C. Gou, and W. C. Wu, Phys. Rev. A **84**, 023610 (2011).